Available online at www.sciencedirect.com
SCIENCE DIRECT
Bioorganic & Medicinal Chemistry
Bioorganic & Medicinal Chemistry 14 (2006) 1546–1557

DFT study of the reductive decomposition of artemisinin

Alex Gutterres Taranto,[a,b] José Walkimar de Mesquita Carneiro[b,c,*] and Martha Teixeira de Araujo[d]

[a]*Departamento de Saúde, Universidade Estadual de Feira de Santana, Feira de Santana, BA, Brazil*
[b]*Programa de Pós-Graduação em Química Orgânica, Universidade Federal Fluminense, Outeiro de São João Batista, s/n, 24020-150, Niterói, RJ, Brazil*
[c]*Departamento de Química Inorgânica, Universidade Federal Fluminense, Outeiro de São João Batista, s/n, 24020-150, Niterói, RJ, Brazil*
[d]*Departamento de Físico-Química, Universidade Federal Fluminense, Outeiro de São João Batista, s/n, 24020-150, Niterói, RJ, Brazil*

Received 19 January 2005; revised 30 August 2005; accepted 4 October 2005
Available online 2 November 2005

Abstract—Artemisinin is a sesquiterpene lactone with an endoperoxide function that is essential for its antimalarial activity. The DFT B3LYP method, together with the 6-31G(d) and 6-31+G(d,p) basis set, is employed to calculate a set of radical anions and neutral species supposed to be formed during the rearrangement of artemisinin from the two radicals (C-centered and O-centered) that are supposed to play a relevant role in the mechanism of action. The B3LYP results show that the primary and the secondary radicals centered on C_4, generated by homolytic break of the C_3–C_4 bond and by 1,5 hydrogen shift, respectively, are more stable than radicals centered on oxygen. The calculations show that the activation barriers for rearrangements are low, leading to a thermodynamically favorable process. These results reinforce our previous conclusions based on semi-empirical calculations but also give additional information on the reductive decomposition of artemisinin.

1. Introduction

Artemisinin (**1**, Fig. 1a) is a sesquiterpene lactone having an endoperoxide bridge that has been in wide use against chloroquine-resistant *Plasmodium falciparum*, one of the agents that cause malaria.[1,2] Artemisinin has a unique 1,2,4-trioxane ring system which has been presumed to be critical to its antimalarial activity, since derivatives lacking the endoperoxide function, e.g., deoxoartemisinin (**2**, Fig. 1b), are inactive.[3,4] The mode of action of artemisinin and its simplified trioxane analogues is still controversial.[5–8] Experimental evidence suggests that endoperoxides may act in the intraerythrocytic stage of parasite development, where they may be activated by heme or free Fe(II) ion, producing potentially cytotoxic free radicals and electrophilic (alkylation) intermediates that may react with and damage specific malaria membrane-associated proteins.[1,8–11]

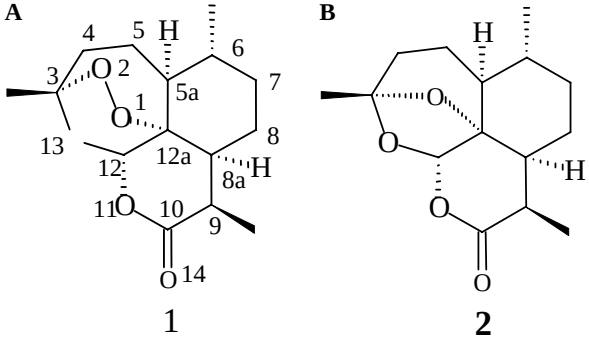

Figure 1. (A) Artemisinin; (B) deoxoartemisinin.

Despite intensive research efforts, a full understanding of the mechanism of action of artemisinin-type compounds at the molecular level has still not been achieved, although several mechanisms have been proposed. Artemisinin could inhibit hemoglobin degradation, the source of aminoacids indispensable for parasite growth.[12] Alternatively, it could interrupt the process of heme detoxification by transferring an

Keywords: Artemisinin; Mechanism of action; DFT.
* Corresponding author. Tel.: +55 21 26292174; fax: +55 21 26292129; e-mail: walk@vm.uff.br

0968-0896/$ - see front matter © 2005 Elsevier Ltd. All rights reserved.
doi:10.1016/j.bmc.2005.10.006

O-atom to heme creating iron-oxene or oxyheme intermediates[13] which would inhibit heme polymerization, or it could act on hemozoin, the insoluble substance formed after digestion of hemoglobin, leading to hemozoin degradation.[12] Both inhibition of heme polymerization and degradation of hemozoin result in heme accumulation in the intraerythrocytic environment.[12] Due to the high toxicity of free heme[14–16] the parasite would be disabled by any of the above processes.

The antimalarial activity of artemisinin may also be due to the trioxane unit acting as a source of hydroperoxide, providing electrophilic oxygenating species, hydroxyl or alkoxyl radicals via reductive cleavage of the peroxide bond by Fe(II) or another reducing agent. These species would be able to hydroxylate biomolecules or abstract hydrogen atoms.[17,18] Reductive cleavage of the endoperoxide bond by electron transfer from heme could also produce potentially cytotoxic oxygen- and carbon-centered radical intermediates.[19–21] Further studies based on the relative potency of substituted derivatives and on artemisinin decomposition catalyzed by the ferrous ion suggested that formation of a secondary carbon-centered radical is of essential importance for high activity.[19–21] This mechanism was further supported by a set of experiments.[10,11,22–33]

In an investigation aimed at unraveling the way artemisinin-type compounds act on the parasite and cause toxicity at the molecular level, we employ the molecular orbital theory to calculate the energy and structures of the main species supposed to be relevant to the mechanism of action of artemisinin.[34–36] Using the semi-empirical AM1 and PM3 methods we have recently calculated a set of radical anions and neutral species that may be formed during the decomposition of artemisinin induced by the addition of one electron to the endoperoxide bridge.[37,38] In the present study, we use the density functional (DFT) approach to undertake a theoretical investigation of the mechanism of reductive decomposition of artemisinin. More specifically we calculate structures and relative energies of intermediates and key transition states involved in the 1,5 hydrogen transfer in artemisinin, a key step in the mechanism of action of this drug.[24] Additionally, we also investigate the barrier for the homolytic cleavage of the C_3–C_4 bond leading to a primary radical centered on C_4. For the first time DFT calculations for this mechanism are reported taking into consideration the complete structure of artemisinin. Although similar calculations on model systems have recently been published,[39] our studies expand the previous one by including the entire artemisinin structure in the calculation as a radical anion, the species which should effectively be responsible for the antimalarial activity.[3,21] For a more complete study we also include similar calculations for protonated artemisinin. Understanding the mechanism of rearrangement of endoperoxides at the molecular level may lead to the rational development of more potent and therapeutically efficient drugs than those already available.

2. Computational methods

The geometries of all species studied in the present work were fully optimized using the Becke's three-parameter hybrid functional,[40] along with the nonlocal correlation functional of Lee, Yang, and Parr (B3LYP).[41,42] The anionic and neutral radicals we calculated have unpaired electrons. For these species the unrestricted formalism (UB3LYP) was employed and a doublet state was specified. The doublet nature of the final optimized structure was confirmed by the expected value of the S^2 operator. Spin contamination was negligible ($S^2 \leqslant 0.756$). The standard 6-31G(d) basis set[43] was employed for geometry optimization and energy calculation. The final relative energy was further refined using the valence split 6-31+G(d,p) basis set[43] which additionally includes diffuse functions on carbon and oxygen atoms, and polarization functions on hydrogens. In this case, the 6-31G(d) optimized geometry was employed. Transition structures were located by defining a reaction coordinate and calculating a set of points along that coordinate. After location of a trial structure, this was further fully optimized by using the standard transition state optimization routine. Harmonic vibrational frequencies were calculated for the transition structure, to confirm it as a true transition state, identified as the structure having only one imaginary vibrational frequency.

For the transition structures IRC (intrinsic reaction coordinate) calculations were carried out to reinforce its nature on the potential energy surface.

All calculations were done with the Gaussian 98W package[44] of molecular orbital program, running on a Pentium II personal computer.

3. Results

Absolute and relative energies are given in Tables 2 and 5. Selected geometrical parameters are given in Table 3. Mulliken net atomic charges and spin densities on selected atoms are given in Tables 1 and 4. The B3LYP/6-31G(d) optimized structures for the anionic radicals are shown in Figures 2 and 4.

3.1. The intramolecular 1,5-hydrogen shift

The most commonly accepted mechanism for the reductive decomposition of artemisinin starts with a single electron transfer from heme or free Fe(II) ion to the endoperoxide bond.[21] Electron-transfer to the peroxide bond results in dissociation of the O–O bond producing an anion and a free radical. In the case of artemisinin two species, **1a** and **1b** (Scheme 1), may be formed. The negative charge may be centered on O_1, with the unpaired electron located on O_2 (**1b**), or vice versa, the negative charge centered on O_2 and the unpaired electron located on O_1 (**1a**). Our calculations show that upon addition of one electron to artemisinin the O_1–O_2 bond breaks up without any activation barrier. Starting from the optimized geometry of artemisinin, after addition of one electron to generate the radical anion, further

Table 1. B3LYP/6-31g(d) Mulliken net atomic charges and spin densities on selected atoms for the radical anions and transition structure involved in 1,5-hydrogen transfer

Structures	O_1	O_2	O_{11}	O_{13}	O_{14}	C_4
Net atomic charge						
1a/1b	−0.561 (−0.410)	−0.489 (−0.636)	−0.479 (−0.476)	−0.556 (−0.466)	−0.518 (−0.448)	−0.290 (−0.349)
TS1	−0.658 (−0.569)	−0.544 (−0.627)	−0.470 (−0.476)	−0.565 (−0.511)	−0.516 (−0.450)	−0.377 (−0.350)
3	−0.739 (−0.670)	−0.691 (−0.636)	−0.474 (−0.473)	−0.563 (−0.515)	−0.515 (−0.451)	−0.153 (−0.243)
Spin densities						
1a/1b	0.448 (0.782)	0.509 (0.006)	0.001 (0.004)	0.008 (0.009)	0.000 (0.003)	0.012 (0.003)
TS1	0.233 (0.469)	0.426 (0.006)	0.000 (0.001)	0.008 (0.000)	0.000 (0.001)	0.356 (0.515)
3	0.011 (0.043)	0.039 (0.023)	0.000 (0.000)	0.011 (0.002)	0.000 (0.000)	1.004 (0.962)

Results in parentheses are for the protonated (neutral) species.

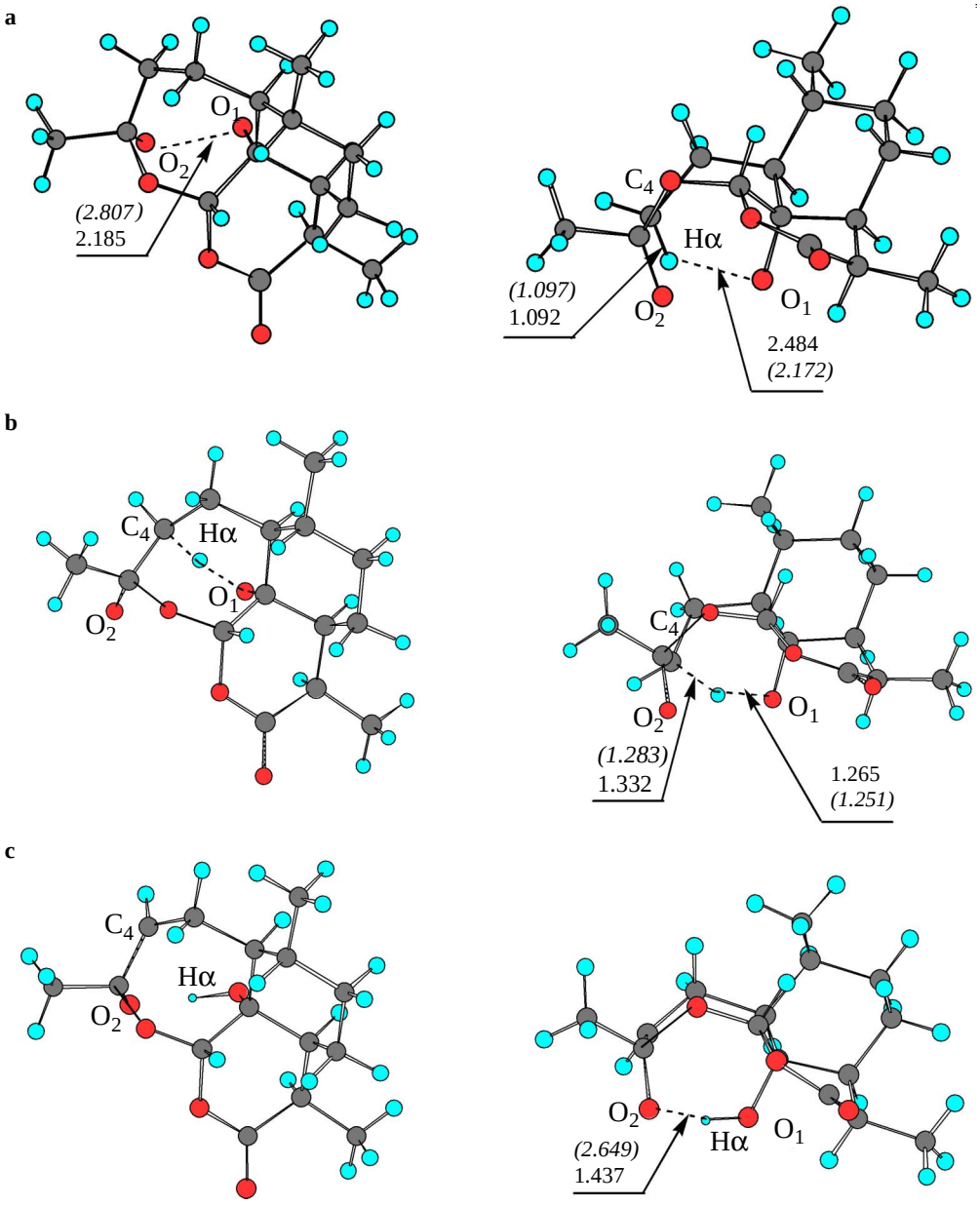

Figure 2. B3LYP/6-31G(d) optimized structures for the anionic radicals (a) the O-centered radical **1a/1b**; (b) the transition structure for the intramolecular 1,5-hydrogen transfer and (c) the C-centered radical. The representation at right clearly indicates the boat-like conformation of these species. Selected distances are given in Å. Values in parentheses are the corresponding distances for the protonated (neutral) species.

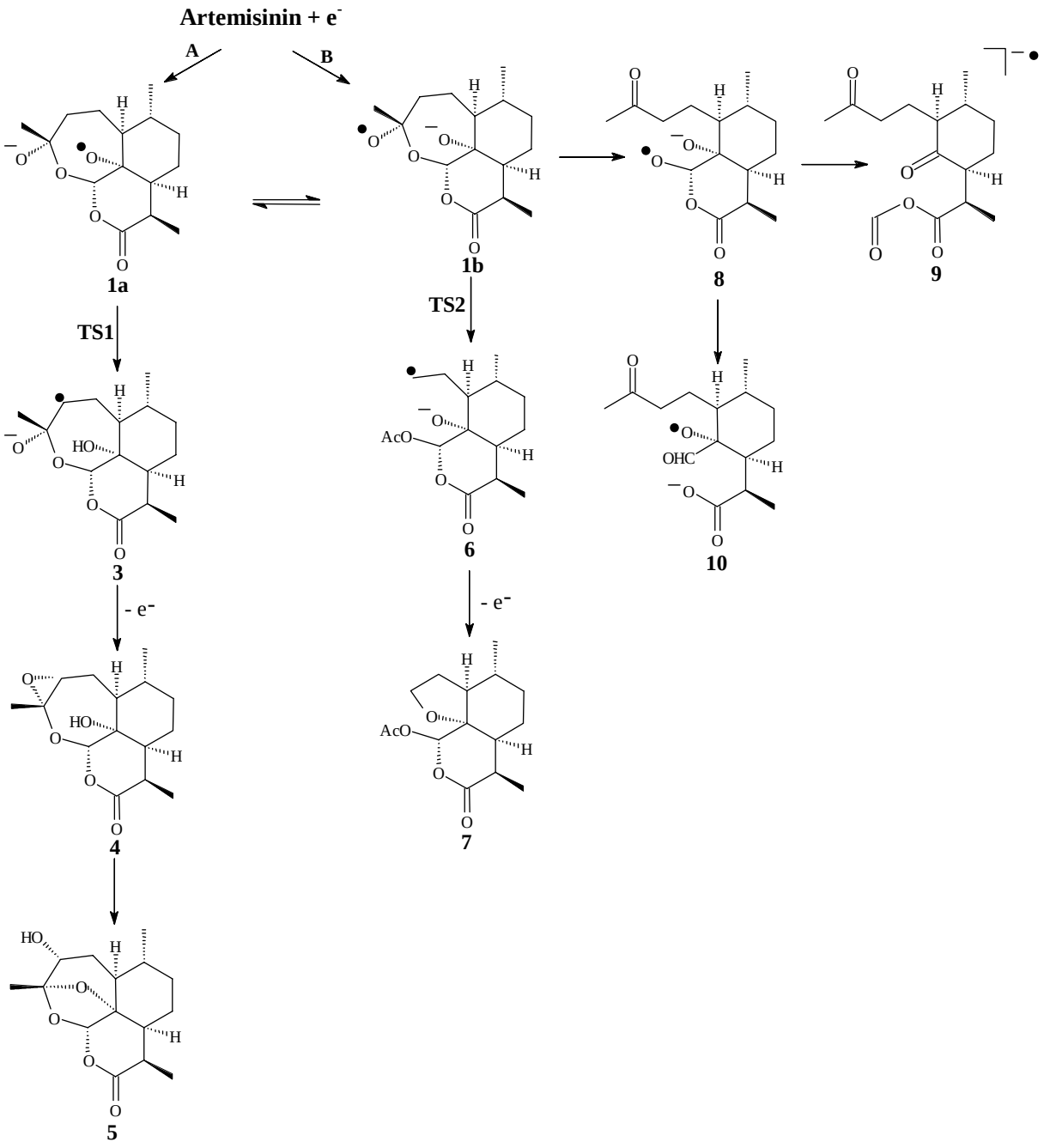

Scheme 1. Possible routes for the reductive decomposition of artemisinin leading to rearranged species.

optimization leads directly to the open structure **1a/1b**. The open nature of **1a/1b** is evident by the O_1–O_2 distance of 2.185 Å (Fig. 2a). **1a/1b** have net atomic charge and spin density distributed almost evenly between the two oxygen atoms (O_1 and O_2), with higher charge on O_1 and higher spin density on O_2 (Table 1). Therefore, the first species in the rearrangement of artemisinin is best described as a resonant hybrid between the two alternating forms, **1a** and **1b**. Consequently, two alternatives have been proposed as possible routes for conversion of artemisinin into its metabolites,[21] either a 1,5-hydrogen transfer from C_4 to O_1, leading to a secondary carbon-centered radical (**3**), or breaking off the C_3–C_4 bond, leading to a primary carbon-centered radical (**6**). In the first mechanism, the crucial step is the rearrangement of **1a** into the secondary carbon-centered radical **3** by an intramolecular 1,5-hydrogen shift.

The B3LYP/6-31G(d) activation energy for the 1,5-hydrogen shift is 23.62 kcal/mol. As expected, addition of diffuse functions on heavy atoms and polarization function on hydrogens (6-31+G(d,p)) reduces the relative energy of the hydrogen bridged transition structure (TS1) to 19.82 kcal/mol (Table 2). Although we did not correct our final activation barrier for either variation in zero-point vibrational energy or entropic effects, the fi-

nal activation energy should not be too different from that calculated in the present study. Corrections for zero-point vibrational energy followed by inclusion of entropic effects reduced the activation barrier in the case of model compounds by only 0.9 kcal/mol.[39] Even if a similar correction is applied to our results, the final activation barrier will be reduced to no less than 19 kcal/mol. This value drastically contrasts to the 6.4 kcal/mol calculated for the model compound.[39] The reason for this evident difference might be in either the geometrical features of the calculated compounds or in the nature of the calculated species (neutral versus anionic). Although the monocyclic model system previously calculated[39] has considerably more flexible geometry than that of artemisinin, this does not seem to be the main origin of the difference between the results for model compounds and artemisinin. In artemisinin, the structure of the transition state may distort to adopt a boat-like conformation (Fig. 2b) favoring the 1,5-hydrogen transfer in an arrangement similar to that calculated for the model compound.

It has been suggested that, due to the high acidity in the parasite's food vacuole, the reaction should happen with a protonated form of artemisinin,[39] i.e., with a neutral radical. Although reaction of artemisinin with $FeSO_4$ in aqueous acetonitrile also yielded essentially the same products as those observed for the in vitro reaction,[21] we decided to calculate the whole mechanism with artemisinin protonated in O_2 (therefore in a neutral form). Results are also given in Tables 1–5.

The results of the calculations with the protonated artemisinin show a considerable reduction in the activation energy for the hydrogen migration. In the protonated case, this activation energy is only 7.1 kcal/mol (B3LYP/6-31+G(d,p)), as compared to the value of 19.8 kcal/mol (B3LYP/6-31+G(d,p)) calculated for the anionic case. This value confirms the previous estimate of 7 kcal/mol for this activation energy based on the calculation of a model system with the B3LYP/6-31G(d,p) procedure.[39]

A more detailed and comparative analysis of the geometric parameters shows that a drastic geometry reorganization occurs when going from the initial radical anion (**1a/1b**) to the transition state (**TS1**). The boat-like conformation is still more pronounced in the transition structure (Fig. 2b). The O_1–$H_{4\alpha}$ distance decreases from 2.484 Å in **1a/1b** to 1.265 Å in **TS1**. The corresponding C_4–$H_{4\alpha}$ distance increases from 1.092 to 1.332 Å. The value of the $C_4H_{4\alpha}O_1$ angle is 149°, close to that calculated by Leszczynski (145°).[39] These results reinforce the hypotheses of Wu et al. that the C–H–O arrangement in the transition structure does not necessarily need to be linear.[21] The boat-like conformation of the

Table 2. Absolute (a.u.) and relative (kcal/mol) B3LYP energies of the anionic and neutral radicals involved in 1,5 hydrogen transfer. The B3LYP/6-31G(d) basis set was used for geometry optimization and the B3LYP/6-31+G(d,p) basis set was used for energy calculation

Structures	B3LYP/6-31G(d)		B3LYP/6-31+G(d,p)	
	Absolute energy (a.u.)	ΔE (kcal/mol)	Absolute energy (a.u.)	ΔE (kcal/mol)
1a/1b	−960.94222 (−961.50662)	0.00 (0.00)	−961.01813 (−961.54262)	0.00 (0.00)
TS1	−960.90459 (−961.49198)	23.62 (9.19)	−960.98655 (−961.53129)	19.82 (7.11)
3	−960.94828 (−961.50658)	−3.80 (0.02)	−961.03284 (−961.54667)	−9.23 (−2.54)

Values in parentheses are for the corresponding protonated species.

Table 3. Selected B3LYP/6-31G(d) distances (Å) for **1a/1b**, **3** and the transition structure **TS1**

Structures	O_1–$H_{4\alpha}$	C_4–$H_{4\alpha}$	O_2–$H_{4\alpha}$	C_3–O_{13}
1a/1b	2.484 (2.172)	1.092 (1.097)	2.431 (2.487)	1.520 (1.461)
TS1	1.265 (1.251)	1.332 (1.283)	2.294 (2.467)	1.554 (1.449)
3	1.060 (0.978)	2.443 (2.022)	1.437 (2.649)	1.582 (1.449)

Values in parentheses are for the corresponding neutral radicals.

Table 4. B3LYP/6-31G(d) Mulliken net atomic charges and spin densities on selected atoms for the radical anions and transition structure for the species involved in the C_3–C_4 break bond

Structures	O_1	O_2	O_{11}	O_{13}	O_{14}	C_4
Net atomic charge						
1a/1b	−0.561 (−0.690)	−0.489 (−0.363)	−0.479 (−0.477)	−0.556 (−0.510)	−0.518 (−0.499)	−0.290 (0.449)
TS2	−0.669 (−0.701)	−0.487 (−0.463)	−0.475 (−0.471)	−0.522 (−0.489)	−0.514 (−0.499)	−0.323 (−0.306)
6	−0.608 (−0.680)	−0.606 (0.496)	−0.503 (−0.483)	−0.549 (0.455)	−0.519 (−0.496)	−0.314 (−0.297)
Spin densities						
1a/1b	0.448 (0.007)	0.509 (0.791)	0.001 (0.000)	0.008 (0.011)	0.000 (0.000)	0.012 (−0.029)
TS2	0.210 (0.001)	0.234 (0.414)	0.000 (0.000)	0.038 (0.030)	0.000 (0.000)	0.528 (0.556)
6	0.002 (0.009)	0.000 (0.000)	0.000 (0.000)	0.002 (0.001)	0.000 (0.000)	1.071 (1.079)

Results in parentheses are for protonated (neutral) species.

Table 5. Absolute (a.u.) and relative (kcal/mol) B3LYP energies of the anionic and neutral radicals involved in the C_3–C_4 bond cleavage. The B3LYP/6-31G(d) basis set was used for geometry optimization and the B3LYP/6-31+G(d,p) basis set was used for energy calculation

Structures	B3LYP/6-31G(d)		B3LYP/6-31 + G(d,p)	
	Absolute energy (a.u.)	ΔE (kcal/mol)	Absolute energy (a.u.)	ΔE (kcal/mol)
1a/1b	−960.94222 (−961.50547)	0.00 (0.00)	−961.01813 (−961.57081)	0.00 (0.00)
TS2	−960.90459 (−961.49931)	23.81 (3.86)	−960.98320 (−961.56569)	21.92 (3.21)
6	−960.93976 (−961.52165)	1.54 (0.02)	−961.02123 (−961.58924)	−1.94 (−11.56)

Values in parentheses are for the corresponding protonated species.

transition structure favors the 1,5-hydrogen transfer as the carbon atom C_4 and the oxygen atom O_1 come close together in this arrangement.

Geometrical parameters for the protonated species are similar. The O_1–$H_{4\alpha}$ distance decreases from 2.172 Å in **1a/1b**, close to the critical limit of 2.1 Å, to 1.251 in **TS1**, and finally to 0.978 Å in **3**. Correspondingly, the C_4–$H_{4\alpha}$ distance increases from 1.097 Å in **1a/1b** to 1.283 Å in **TS1**, up to 2.022 Å in **3**. However, it should be observed that due to the higher charge density in the anionic species, mainly on O_2, there is a clear approximation of the migrating hydrogen to O_2, the oxygen atom formally bearing the negative charge. In the product (**3**), the O_2–$H_{4\alpha}$ distance is only 1.437 Å. In contrast, in the neutral case, $H_{4\alpha}$ is almost equidistant from O_2 in all the structures (**1a/1b**, **TS1** and **3**). Another structural parameter that called our attention is the C_3–O_{13} distance. Interestingly, this distance is significantly larger in the anionic than in the neutral case. In the neutral species, the C_3–O_{13} distance is almost constant, similar to the values usually found in a single C–O bond. However, in the anionic case there is a continuous increase in that bond, going from 1.520 Å in **1a/1b**, up to 1.582 Å in **3**. This value is much larger than those found in common single C–O bonds (about 1.45 Å). In our opinion, the enlargement in this C–O bond is the main origin of the higher activation energy for the anionic species as compared to that in the neutral one.

The calculation of harmonic vibrational frequencies revealed that **TS1** is a true transition state and indicated the atoms undergoing the main displacement in the transition structure. The arrows representing the vibrational mode corresponding to the imaginary frequency in the

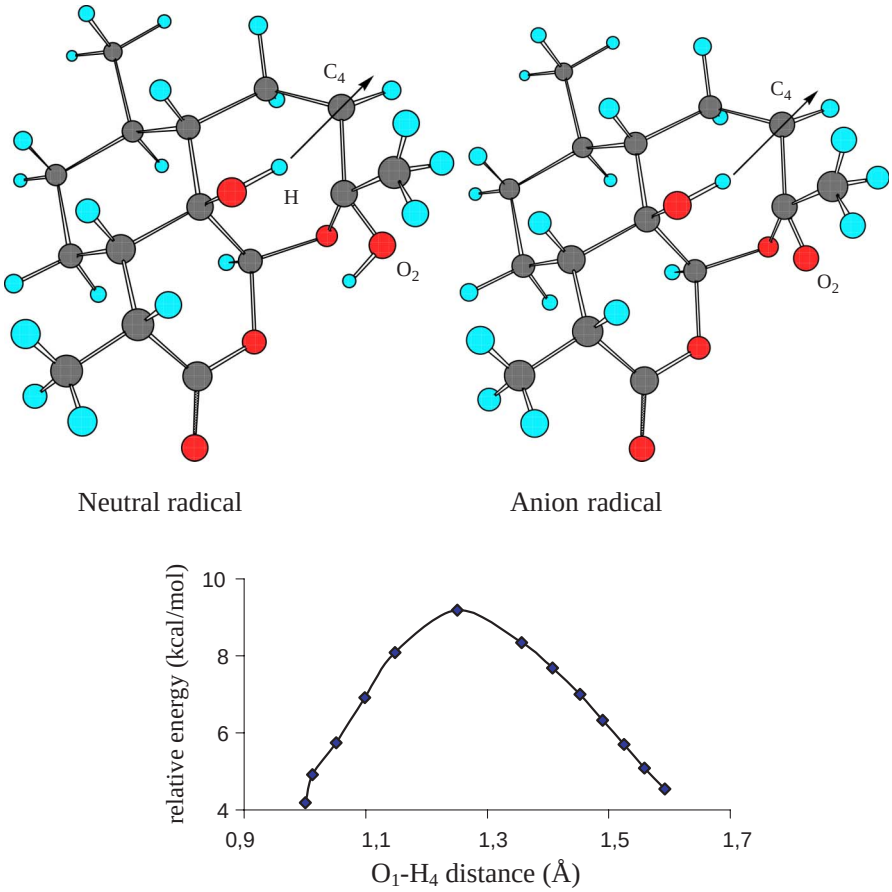

Figure 3. The potential energy surface for the intramolecular 1–5 hydrogen shift in the protonated structure. The arrows represent the vibration mode corresponding to the imaginary frequency of 1494i cm^{-1} in the transition state of the neutral species and 1513i cm^{-1} for the anionic radical.

transition structure are shown in Figure 3. Although this involves mainly displacement of the migrating hydrogen atom, this movement is strongly coupled with the cleavage of the C_3–O_{13} bond. Successive attempts to run IRC calculations for the anionic case, starting from the transition structure **TS1**, were not successful. All attempts resulted in an unconverged or unsatisfactory structure. We could predict however that the migration of the hydrogen atom in the anionic case is strongly coupled with breaking off the C_3–O_{13} bond. Possible intermediates formed in this pathway are shown in Scheme 2. As shown, the rearrangement of artemisinin by the cleavage of the C_3–O_{13} bond leads to stable structures, where the unpaired electron and the negative charge are far away from each other, both stabilized by electron delocalization. Formation of an intermediate similar to **12** has already been suggested on the basis of experimental studies.[21] In the case of the neutral species, the formation of a double bond between C_3 and O_2 is hampered, avoiding thereafter the break of the C_3–O_{13} bond. In contrast to the anionic case, where the IRC calculation does not run satisfactorily, IRC calculations for the transition structure of the neutral radical, as shown in Figure 3, confirmed that species as the true transition state connecting **1a/1b** and **3**.

The secondary carbon-centered radical **3** has been proposed as a fundamental species in the mechanism of action of artemisinin.[24] This radical would be able to alkylate specific membrane parasite proteins.[24] Previous B3LYP calculations on model compounds indicate that **3** is only slightly more stable than the initial radical **1a/1b**, while the semi-empirical AM1 and PM3 methods predicted it to be much more stable.[37] The present B3LYP/6-31+g(d,p)//B3LYP/6-31g(d) relative energy reproduces the previous B3LYP calculations, indicating **3** to be 9.2 kcal/mol more stable than **1a/1b** in the anionic species. This energy difference is reduced to 2.5 kcal/mol in the case of the neutral species, still favoring **3** over **1a/1b**. In the secondary radical **3**, the carbon atom C_4 has a spin density of about 0.9–1.0 in both the anionic and the neutral cases, indicating that the unpaired electron is essentially located on C_4. Spin densities on the oxygen atoms are reduced to essentially zero (Table 1), while charge density is almost evenly distributed among the oxygen atoms (Table 1). Charge distribution in **TS1** is similar to that calculated for **3**, with charge distributed among all the oxygen atoms. Spin densities in **TS1** clearly indicate that there is a transfer of spin from O_2 to C_4 in the anionic case, and from O_1 to C_4 in the neutral case, as indicated by an increase in spin density on C_4 going from **1a/1b** to **TS1** with a simultaneous reduction in spin density on either O_1 or O_2 (Table 1).

3.2. The homolytic cleavage of the C_3–C_4 bond

The homolytic cleavage of the C_3–C_4 bond was also studied in a similar way as done for the 1,5-hydrogen migration. Calculations with the DFT (B3LYP) methodology and the 6-31G(d) and 6-31+G(d,p) basis set were employed to study the details of the C_3–C_4 homolytic break starting from structure **1a/1b**, with formation of a primary radical anion centered on C_4 (**6**). The protonated species were also calculated, as described previously. The intermediate **6** may also play a relevant role in the mechanism of action of artemisinin and other antimalarial endoperoxides, since it has been thought to be responsible for alkylation of heme,[22,23,45,46] a key step in that mechanism.

Starting from **1a/1b** the transition state (**TS2**) for formation of **6** is shown in Figure 4. It has a relative energy of 23.8 kcal/mol in the anionic species and of 3.9 kcal/mol in the neutral case, as compared to that of **1a/1b** (Table 5). Similar to the results found for the 1,5 hydrogen migration, the addition of polarization and diffuse functions reduces this activation energy to 21.9 and 3.2 kcal/mol, respectively, for the anionic and the neutral cases. It is important to observe that, in contrast to the case of the 1,5-hydrogen migration, where protonation occurred in the oxygen atom O_2, in the present case the oxygen atom O_1 was protonated. In both cases, a strong intramolecular hydrogen bond was found in the protonated species. Formation of this hydrogen bond may explain the strong reduction of the activation energy when going from the anionic to the neutral species. Comparing these results to those obtained for the model compounds,[39] we have calculated a lower activation barrier for the neutral case, although the activation energy for the anionic case is considerably higher, as was found for the 1,5 hydrogen migration.

Harmonic vibrational frequency calculation confirms the transition structure (**TS2**) as a true transition state with a unique imaginary vibrational frequency for both the anionic ($-454.9\ cm^{-1}$) and the neutral species

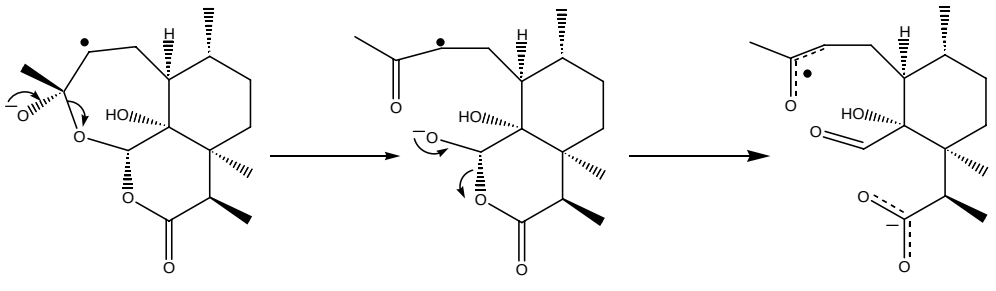

Scheme 2. Possible intermediates formed during the rearrangement of the secondary C_4-centered radical after cleavage of the C_3–O_{13} bond.

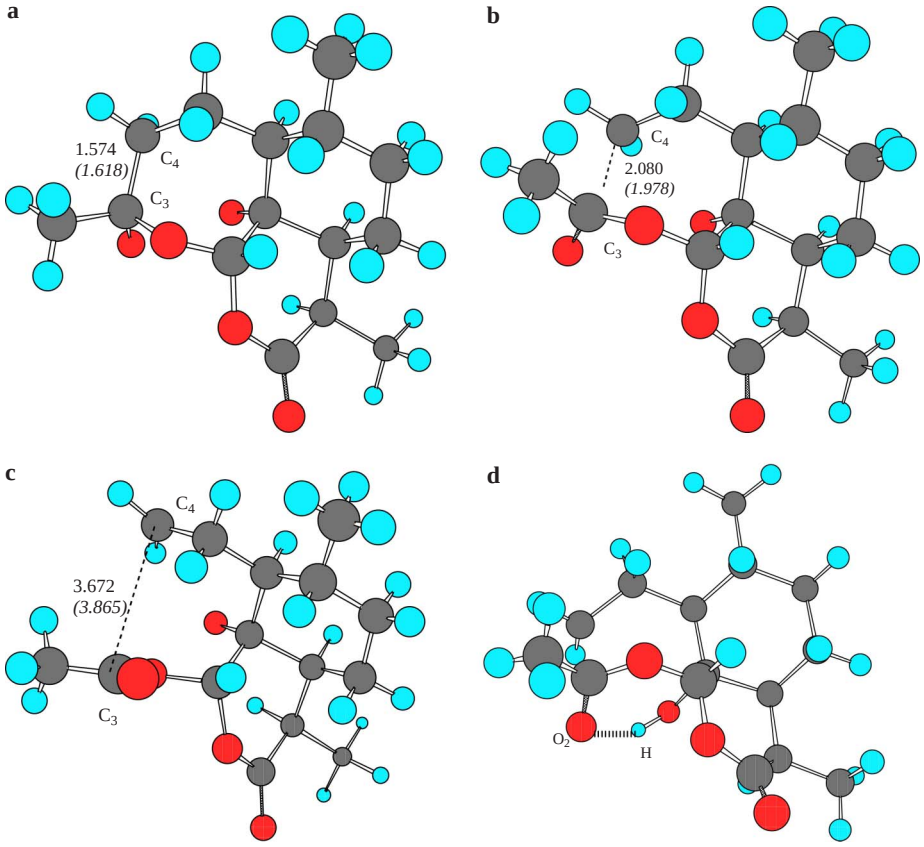

Figure 4. (a) Optimized structure for the O-centered radical **1a/1b**; (b) the transition state for the C_3–C_4 bond break (**TS2**); (c) optimized structure **6**; (d) hydrogen bond between the hydrogen atom bonded to O_1 and the oxygen atom O_2 in neutral transition state (**TS2**). The distances are in Å. The values in parentheses are for the protonated species (neutral).

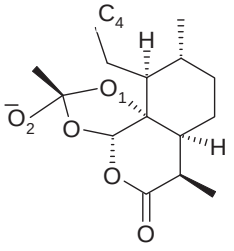

Figure 5. Intermediate **6a**. The hydrogens were omitted for better visualization.

($-429.4\ cm^{-1}$). IRC calculations starting from this transition structure (Fig. 6) confirmed that this connects the reagent structure **1a/1b** to the intermediate structure **6**.

The spin densities on relevant atoms clearly show that the C_3–C_4 bond breaks homolytically (Table 4). Carbon atom C_4 in structure **1a/1b** has essentially null spin density (0.012). In the transition structure (**TS2**), this value increases to 0.528 and finally in structure **6** the unpaired electron is completely centered on C_4, with a spin density of 1.071. A similar behavior is calculated for the neutral form, the spin density on C_4 in **1a/1b** is initially zero, increasing to an intermediate value in the transition state (0.556), and ending with a spin density of 1.079 in structure **6**, similar to the values found with the semi-empirical methods. Charge densities (Table 4) suffer significant variation only in the transition state (**TS2**), being more intense on O_1.

Geometric details of the C_3–C_4 cleavage are shown in Figure 4. The initial C_3–C_4 distance is 1.574 Å in **1a/1b** increasing to 2.080 Å in the transition state (**TS2**). In the product, this bond has completely broken, having a final distance of 3.672 Å. For the neutral species, the behavior is similar. The C_3–C_4 distance, increases from 1.618 Å in structure **1a/1b**, to 1.978 Å in the transition state, reaching 3.865 Å in the final structure. These values are similar to those computed before for model compounds.[39] Leszczynsky also found an additional minimum energy structure on the potential energy surface with 4.99 Å for the distance between C_3 and C_4. A similar structure, with a longer C_3–C_4 distance has also been located in the present study. However, the key point in the process is the activation barrier to break the C_3–C_4 bond, generating the primary radical. Our calculations also show that the anionic form of **6** may spontaneously rearrange into a structure that has never been described before (**6a**). This is 12.43 kcal/mol more stable than the structure proposed previously.[19–21,24,39] This new intermediate is formed by nucleophilic attack of O_1 on the carbonyl carbon C_3 leading to a five-membered ring, where the highest negative charge is found on O_2 (Fig. 5). The neutral form of **6** cannot rearrange into the five-membered-ring because O_1 is protonated, therefore having its nucleophilicity strongly reduced.

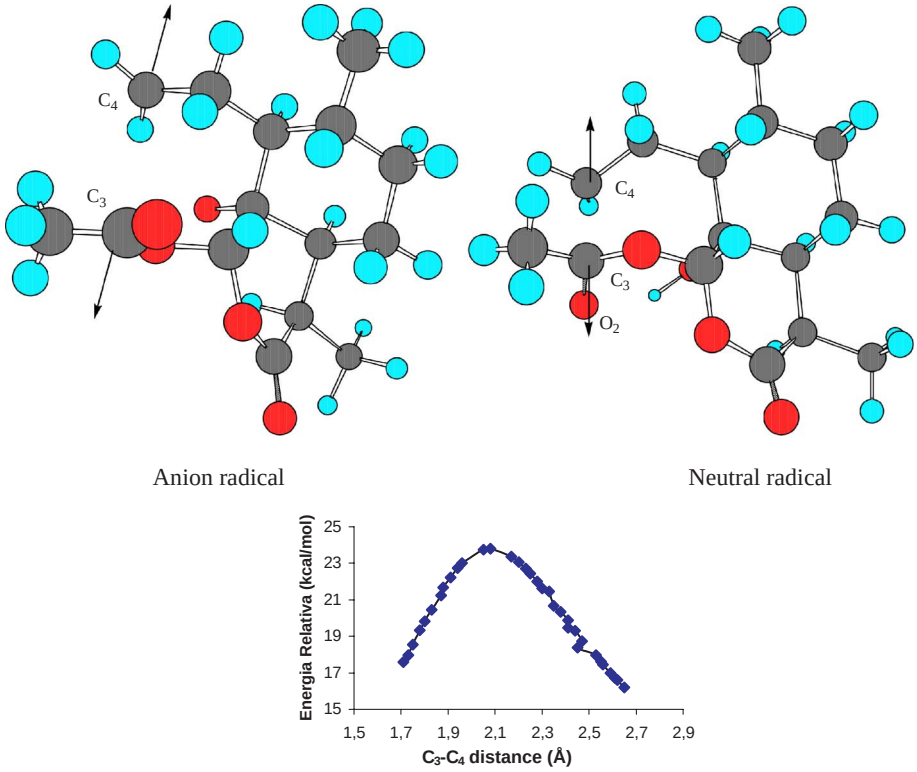

Figure 6. The potential energy surface for the homolytic C_3–C_4 cleavage in the protonated structure. The arrows represent the vibration mode corresponding to the imaginary frequency of 454.9i cm^{-1} in the transition state of for the anionic radical and 429.4i cm^{-1} for the neutral species.

3.3. Additional structures

Another key intermediate that has been proposed to play some role in the mechanism of action of artemisinin is an epoxide form (see **4**, Scheme 1). Due to its high alkylating property,[19,20] it was considered by Posner as probably responsible for the death of the parasite.[19,20] However, this was contested by Avery who synthesized some endoperoxides with an epoxide group and showed that they do not have any antimalarial activity.[47] The effective identification of the epoxide as a possible intermediate in the degradation of artemisinin was achieved by Wu et al., who isolated an epoxide derivative among the products of decomposition of artemisinin induced by ferrous ion, albeit at low yield (1–2%).[21] Our B3LYP calculations reinforce the previous semi-empirical results[37]. Although a direct comparison of the relative stability of the epoxide form to the other structures discussed before is not possible, the data indicate that it is probably too unstable to play any role in the mechanism. This conclusion is based on the energy difference between the epoxide **4** and the alcohol **5**, which may be obtained from **4** by nucleophilic attack of oxygen O_1 on the carbon atom C_3, followed by the opening of the epoxide ring and hydrogen migration. According to B3LYP/6-31G(d) structure **5** is 32.2 kcal/mol more stable than **4** (the corresponding semi-empirical value is of the order of 40 kcal/mol). Although we could not locate a transition structure leading from **4** to **5**, the large energy difference between these structures indicates that the activation energy to decomposition of the epoxide form should be considerably low.

We also investigated structure **8**. This may be obtained from **1a/1b** by homolytic cleavage of the C_3–O_{13} bond, in a process similar to that discussed before, although in that case the break of the C_3–O_{13} bond occurred in a concerted way with 1,5-hydrogen transfer, as previously discussed. Successive attempts to locate **8** were not successful. All optimizations always led directly to the fully rearranged form **9**. In this species, both the charge and spin densities are completely distributed among the several oxygen atoms. In another way, structure **10** may also be formed. Similar to **9**, **10** has charge and spin densities that are fully distributed among the oxygen atoms. However, contrary to previous proposals,[21] charge is more concentrated on the carboxyl group, while spin densities concentrate on the oxygen O_1. These rearranged forms are considerably more stable than any of the initial intermediates.

4. Discussion

The results of the present work clearly show that artemisinin undergoes reductive decomposition in an exothermic process which leads to rearranged products that are much more stable than the starting materials. Formation of the initial O-centered radical occurs without any activation energy. In this radical charge and spin densities indicate that it is better described as a hybrid that may be represented by the resonant structures **1a** and **1b**. 1,5-hydrogen migration converts this O-centered radical into the more stable C-centered

radical (**3**), with an activation energy that is strongly dependent on the charge on the calculated species. For anionic radicals the activation energy is of the order of 19 kcal/mol. This activation energy is drastically reduced to about 7 kcal/mol when neutral, protonated species are considered. In the case of anionic radicals, the 1,5-hydride transfer is strongly coupled with the C_3–O_{13} bond break, this being the main origin for the high activation energy. Breaking the C_3–O_{13} bond leads to an intermediate (**9**) where the negative charge and the unpaired electron are both stabilized by electron delocalization.

The O-centered radical may also rearrange into a primary radical (**6**) by cleavage of the C_3–C_4 bond. This primary radical is also calculated to be slightly more stable than the O-centered radical although less stable than the secondary C-centered radical. Activation energy to form the primary radical (22 kcal/mol) is of the same magnitude as that calculated for formation of the secondary radical (19 kcal/mol), therefore both processes may be observed under experimental conditions, although the probability of formation of the secondary radical should be considerably higher due to its higher thermodynamic stability.

Reduction of the activation energy in the protonated neutral case favors the cleavage of the C_3–C_4 bond. In this case, the relative energy of the transition structure **TS2** is about 4 kcal/mol lower than that of the alternative structure **TS1**. Correspondingly, the protonated primary C-centered radical (**6**) has a relative energy of about 9 kcal/mol lower than that of the protonated secondary C-centered radical (**3**). Breaking the C_3–C_4 σ bond leads to formation of a stable carboxylate that helps stabilize both the transition structure and the intermediate.

Metabolites presumably formed in both pathways were isolated under experimental conditions.[21] These experimental observations give support to our results that activation energy to form the primary and the secondary radicals is essentially equivalent, although slightly lower for formation of the secondary radical in the case of the anionic species and considerably lower for formation of the primary radical in the case of the protonated neutral species. It has been suggested that the only species that is able to alkylate biomolecules is the primary radical **6**.[21]

The function of the carbon-centered radicals in the mechanism of action of artemisinin has been questioned, particularly the 1,5-hydrogen transfer.[13] The main argument against the 1,5 hydride migration is the great distance between the hydrogen on C_4 and the oxygen O_1 in structure **1a/1b**.[13] This distance is 2.484 Å for the anionic radical and 2.172 Å for the neutral one. However, the orientation of the α hydrogen on C_4 is favorable for the migration since the seven-membered ring of **1a/1b** may assume a boat-like conformation that helps in the transfer process. The importance of the 1,5 hydrogen migration was strengthened by Posner, who showed that substitutions in C_4 can modulate the antimalarial activity of several analogous.[39] Alkyl groups

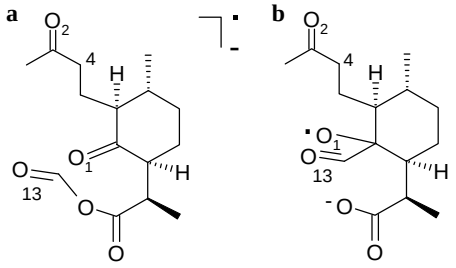

Figure 7. (a) Strucutre **9**; (b) Structure **10**. The hydrogens are omitted in both figures for better visualization.

substituted in $C_{4\beta}$ favor the formation of the radical in C_4 and increase the antimalarial activity. In contrast, substitution of the C4α hydrogen disfavors the formation of radicals centered on C_4 and decreases the antimalarial activity. It may be observed, however, that substituents $C_{4\beta}$ that strongly stabilize the tertiary radical (silicon compounds for example) lead to reduced antimalarial activity as compared to compounds not substituted in C_4.[39] It was implied that the antimalarial activity depends on an ideal imbalance between stability and reactivity.[47] A more detailed discussion on this topic was given elsewhere.[36]

Due to its powerful alkylating property, the epoxide intermediate **4** was considered[19,20] as a possible inductor for the activity of artemisinin. However, its high relative energy leads to a too low intrinsic stability, which most probably precludes it of being able to participate in the mechanism as a key intermediate. For example, it may easily be converted to secondary products by means of acidic catalysis. Structure **5**, which may result from rearrangement of **4**, is considerably more stable. In this way, once formed **4** should have a short lifetime. Synthetic epoxides, structurally related to **4**, are inactive.[47]

Our results indicate that the carbon-centered radicals are the most probable candidates for the species playing the most relevant role in the mechanism of action of artemisinin, in agreement with previous experimental findings.[47] The C-centered radicals are more stable than the corresponding O-centered ones, according to the whole exothermic process. Additional rearrangement products also have low relative energy, however these may be attained only through relatively high activation energies (see Fig. 7).

5. Conclusions

In this paper, we present high level DFT calculations for the mechanism of reductive decomposition of artemisinin. In special we concentrate on the 1,5-hydrogen transfer and on the C_3–C_4 bond cleavage, either in an anionic radical or in a neutral form. Activation energy for the 1,5-hydrogen transfer strongly depends on the nature of the calculated species. For the anionic radicals an activation energy of 19.8 kcal/mol was calculated. In contrast, for the neutral radicals a barrier of 7.1 kcal/mol is calculated. This value is similar to those calculat-

ed before for a model system using a similar methodology. The migration of the hydrogen atom in the anionic species is strongly coupled with the breakdown of the C_3–O_{13} bond, which may be the main origin for the higher activation energy calculated in this case. This leads to products where the unpaired electron and the negative charge are both stabilized by electron delocalization, although far away from each other in the structure. Similarly, the C_3–C_4 bond breaks with an activation energy of 22 kcal/mol in the anionic radical, while for the neutral case a barrier of only 3.2 kcal/mol is calculated. In all cases, the carbon-centered radicals are more stable than the corresponding oxygen-centered radicals. From these results we can conclude that the rearrangement of the reduced form of artemisinin is a fast process in a protic medium or in a medium where a counterion may strongly interact with it, for example, by complexing artemisinin with heme. In contrast, in a medium where the anionic form of artemisinin remains unencumbered it may survive for a longer time, perhaps enough for the species with an O-centered radical to have some activity. Additional structures were found which have much higher stability, however, they are obtained only by pathways with relatively high activation energies.

Acknowledgments

We acknowledge financial support from CNPq (Proc. No. 478954/2001-8), CAPES, UEFS, and FAPESB.

References and notes

1. Klayman, D. L. *Science* **1985**, *228*, 1049.
2. Frédérich, M.; Dogné, J. M.; Angenot, L.; Mol, P. D. *Curr. Med. Chem.* **2002**, *9*, 1435.
3. Meshinick, S. R.; Taylor, T. E.; Kamchonwongpaisan, S. *Microb. Rev.* **1991**, *60*, 301.
4. Luo, X. D.; Shen, C. C. *Med. Res. Rev.* **1987**, *07*, 29.
5. Olliaro, P. L.; Haynes, R. K.; Meunier, B.; Yuthavong, Y. *Trends Parasitol.* **2001**, *17*, 122.
6. Posner, G.; Meshnick, S. R. *Trends Parasitol.* **2001**, *17*, 266.
7. Olliaro, P. L.; Haynes, R. K.; Meunier, B.; Yuthavong, Y. *Trends Parasitol.* **2001**, *17*, 267.
8. Kamchonwongpaisan, S.; Meshinick, S. R. *Gen. Pharmac.* **1996**, *27*, 587.
9. Bhisutthibban, J.; Pan, X. Q.; Hossler, P. A.; Walker, D. J.; Yowell, C. A.; Carlton, J.; Dame, J. B.; Meshnick, S. R. *J. Biol. Chem.* **1998**, *272*, 16192.
10. Meshinick, S. R.; Thomas, A.; Ranz, A.; Xu, C. M.; Pan, H. Z. *Mol. Biochem. Parasitol.* **1991**, *49*, 181.
11. Yang, Y. Z.; Little, B.; Meshinick, S. R. *Biochem. Pharmacol.* **1994**, *48*, 569.
12. Pandey, A. V.; Tekwani, B. L.; Singh, R. L.; Chauhan, V. S. *J. Biol. Chem.* **1999**, *274*, 19383.
13. Jefford, C. W.; Favager, F.; Vicente, M. G. H.; Jacquier, Y. *Helv. Chim. Acta* **1995**, *78*, 452.
14. Fitch, C. D.; Chevli, R.; Banyal, H. S.; Phillips, G.; Pfaller, M. A.; Krogstad, D. *Antimicrob. Agents Chemother.* **1982**, *21*, 819.
15. Pandey, A. V.; Tekwani, B. L. *FEBS Lett.* **1997**, *402*, 236.
16. Zhang, J.; Krugliak, M.; Ginsburg, H. *Mol. Biochem. Parasitol.* **1999**, *99*, 129.
17. Haynes, K. H.; Pai, H. H. O.; Voerste, A. *Tetrahedron Lett.* **1999**, *40*, 4715.
18. Haynes, K. H.; Vonwiller, S. C. *Tetrahedron Lett.* **1996**, *37*, 253.
19. Posner, G. H.; Cumming, J. N.; Ploypradith, P.; Oh, C. H. *J. Am. Chem. Soc.* **1995**, *117*, 5885.
20. Posner, G. H.; Park, S. B.; González, L.; Wang, D.; Cumming, J. N.; Klinedinst, D.; Shapiro, T. A.; Bachi, M. D. *J. Am. Chem. Soc.* **1996**, *118*, 3537.
21. Wu, W. M.; Wu, Y.; Wu, Y. L.; Yao, Z. J.; Zhou, C. M.; Li, Y.; Shan, F. *J. Am. Chem. Soc.* **1998**, *120*, 3316.
22. Robert, A.; Meunier, B. *J. Am. Chem. Soc.* **1997**, *119*, 5968.
23. Robert, A.; Meunier, B. *Chem. Soc. Rev.* **1998**, *27*, 273.
24. Cumming, J. N.; Wang, D.; Park, S. B.; Shapiro, T. A.; Posner, G. H. *J. Med. Chem.* **1998**, *41*, 952.
25. Oh, C. H.; Posner, G. H. *J. Am. Chem. Soc.* **1992**, *114*, 8328.
26. Posner, G. H.; Oh, C. H.; Wang, D.; Gerena, L.; Milhous, W. K.; Meshnick, S. R.; Asawamahasadka, W. *J. Am. Chem. Soc.* **1994**, *37*, 1256.
27. Kapetanaki, S.; Varotsis, C. *FEBS Lett.* **2000**, *474*, 238.
28. Asawamahasadka, W.; Ittrat, I.; Pu, Y. M.; Ziffer, H.; Meshnick, S. *Antimicrob. Agents Chemother.* **1994**, *38*, 1854.
29. Zhang, F.; Gosser, D. K., Jr.; Meshnick, S. R. *Biochem. Pharmacol.* **1992**, *43*, 1805.
30. Meshnick, S. R.; Yang, Y. Z.; Lima, V.; Kuypers, F.; Kamchonwongpaisan, S.; Yuthavong, Y. *Antimicrob. Agents Chemother.* **1993**, *37*, 1108.
31. Butler, A. R.; Gilebert, B. C.; Hulme, P.; Irvine, L. R.; Renton, L.; Whitwood, A. *Free Rad. Res.* **1998**, *28*, 471.
32. Wu, Y. *Acc. Chem. Res.* **2002**, *35*, 255.
33. Meshnick, S. R. *Int. J. Parasitol.* **2002**, *32*, 1655.
34. Taranto, A. G.; Carneiro, J. W. de M.; Oliveira, F. G. *J. Mol. Struct. (Theochem)* **2001**, *539*, 267.
35. Konishi, T. N.; Taranto, A. G.; Carneiro, J. W. de M. *Eur. J. Pharm. Sci.* **2001**, *13*(Suppl. 1), S122.
36. Arantes, C.; Araujo, M. T.; Taranto, A. G.; Carneiro, J. W. M. *Int. J. Quant. Chem.* **2005**, *103*, 749.
37. Taranto, A. G.; Carneiro, J. W. de M.; Oliveira, F. G.; Araujo, M. T.; Correa, C. R. *J. Mol. Struct. (Theochem)* **2002**, *580*, 207.
38. Taranto, A. G.; Carneiro, J. W. M.; Araujo, M. T. *Braz. J. Pharm. Sci.* **2003**, *39*(Suppl. 2), 180.
39. Gu, J.; Chen, K.; Jiang, H.; Leszczynski, J. *J. Phys. Chem. A* **1999**, *103*, 9364.
40. Becke, A. D. *J. Chem. Phys.* **1993**, *98*, 5648.
41. Lee, C.; Yang, W.; Parr, R. G. *Phys. Rev. B* **1988**, *37*, 785.
42. Vosko, S. H.; Wilk, L.; Nusair, M. *Can. J. Phys.* **1980**, *58*, 1200.
43. Hehre, W. J.; Radom, L.; Schleyer, P. v. R.; Pople, J. A. *Ab Initio Molecular Orbital Theory*; Wiley: New York, 1986.
44. Gaussian 98 Revision A.7, Frisch, M. J.; Trucks, G. W.; Schlegel, H. B.; Scuseria, G. E.; Robb, M. A.; Cheeseman, J. R.; Zakrzewski, V. G.; Montgomery, J. A. Jr.; Stratmann, R. E.; Burant, J. C.; Dapprich, S., Millam, J. M.; Daniels, A. D.; Kudin, K. N.; Strain, M. C.; Farkas, O.; Tomasi, J.; Barone, V.; Cossi, M.; Cammi, R.; Mennucci, B.; Pomelli, C.; Adamo, C.; Clifford, S.: Ochterski, J.; Petersson, G. A.; Ayala, P. Y.; Cui, Q.; Morokuma, K.; Malick, D. K.; Rabuck, A. D.; Raghavachari, K., Foresman, J. B.; Cioslowski, J.; Ortiz, J. V.; Baboul, A. G.; Stefanov, B. B.; Liu, G.; Liashenko, A.; Piskorz, P.; Komaromi, I.; Gomperts, R.; Martin, R. L.; Fox, D. J.; Keith, T.; Al-Laham, M. A.; Peng, C.

Y.; Nanayakkara, A.; Gonzalez, C.; Challacombe, M.; Gill, P. M. W.; Johnson, B.; Chen, W.; Wong, M. W.; Andres, J. L.; Gonzalez, C.; Head-Gordon, M.; Replogle, E. S.; Pople, J. A.; Gaussian Inc., Pittsburgh, PA, 1998.

45. Provot, O.; Dedenis, B. C.; Hamzaoui, M.; Moskwitz, H.; Mayrargue, J.; Robert, A.; Cazelles, J.; Meunier, B.; Zouhiri, F.; Desmaële, D.; Angelo, J.; Mauhteau, J.; Gay, F.; Cicéron, L. *Eur. J. Org. Chem.* **1999**, 1935.
46. Cazelles, J.; Dedenis, B. C.; Provot, O.; Robert, A.; Mayrargue, J.; Meunier, B. *J. Chem. Soc. Perkin Trans. 1* **2000**, 1265.
47. Avery, M. A.; Fan, P.; Karle, J. M.; Bonk, J. D.; Miller, R.; Goins, D. K. *J. Med. Chem.* **1996**, *39*, 1885.